Helical Structure of Dermaseptin B2 in a Membrane-Mimetic Environment

Olivier Lequin,[‡] Francine Bruston,[§] Odile Convert,[‡] Gérard Chassaing,[‡] and Pierre Nicolas*[,§]

UMR 7613 CNRS, Université Paris 6, Structure et fonction de molécules bioactives, Université Pierre et Marie Curie, Case Courrier 45, 4 Place Jussieu, 75252 Paris Cedex 05, France, and UMR 7592 CNRS, Universités Paris 6 et 7, Laboratoire de Bioactivation des Peptides, Institut Jacques Monod, 2 Place Jussieu, 75251 Paris Cedex 05, France

Received March 12, 2003; Revised Manuscript Received May 28, 2003

ABSTRACT: Dermaseptins are antimicrobial peptides from frog skin that have high membrane-lytic activity against a broad spectrum of microorganisms. The structure of dermaseptin B2 in aqueous solution, in TFE/water mixtures, and in micellar and nonmicellar SDS was analyzed by CD, FTIR, fluorescence, and NMR spectroscopy combined with molecular dynamics calculations. Dermaseptin B2 is unstructured in water, but helical conformations, mostly in segment 3−18, are stabilized by addition of TFE. SDS titration showed that dermaseptin B2 assumes nonhelical structures at SDS concentrations far below the critical micellar concentration and helical structures at micellar concentrations. Dermaseptin B2 bound to SDS micelles (0.4 mM peptide, 80 mM SDS) adopts a well-defined amphipathic helix between residues 11−31 connected to a more flexible helical segment spanning residues 1−8 by a flexible hinge region around Val9 and Gly10. Experiments using paramagnetic probes showed that dermaseptin B2 lies near the surface of SDS micelles and that residue Trp3 is buried in the SDS micelle, but close to the surface. A slow exchange equilibrium occurs at higher peptide/SDS ratios (2 mM peptide, 80 mM SDS) between forms having distinct sets of resonances in the N-terminal 1−11 segment. This equilibrium could reflect different oligomeric states of dermaseptin B2 interacting with SDS micelles. Structure−activity studies on dermaseptin B2 analogues showed that the N-terminal 1−11 segment is an absolute requirement for antibacterial activity, while the C-terminal 10−33 region is also important for full antibiotic activity.

Many membrane-lytic peptides permeate the bacterial cell membrane and cause cell death. The most abundant in nature are the linear lytic peptides that are believed to assume an amphipathic α-helix structure once they become bound to membranes (*1*). They seem to undergo conformational changes when they reach the target membrane, which enables them to associate with the membrane, provoke its permeabilization, and disrupt it by one of two general postulated mechanisms: (i) transmembrane pore formation via a "barrel-stave" mechanism which holds for cell nonselective peptides and (ii) membrane destruction/solubilization via a "carpet" mechanism for antimicrobial peptides (*2*).

CD[1] spectroscopy (*3*) and, to a limited extent, FTIR, ATR-FTIR (*4*−*6*), and Raman spectroscopy (*7*, *8*) have been used to study the conformation of linear peptide antibiotics in various structure-promoting solvents and membrane-mimetic environments (*9*, *10*). These methods provide an overall picture of the conformation of these peptides, which is a valuable starting point for assessing their helical propensity, but they cannot locate structural motifs within the peptide sequence. In contrast, NMR spectroscopy can yield information about the structure of single residues. However, it has not yet been used extensively to study the conformation of linear amphipathic peptides in membrane or membrane-mimetic environments. The determination of the precise three-dimensional structure of these peptides when they are bound to lipid bilayers and the molecular characterization of their interactions are key steps toward understanding their mechanism of action and analyzing structure−activity relationships.

Dermaseptins (Drs) form a vast family of functionally related peptides that are 24−34 residues long and are produced by the skin of South American hylid frogs (*11*−*15*). They are linear cationic, lysine-rich peptides endowed with membrane-lytic activity against a broad spectrum of microorganisms, including bacteria, yeast (*16*), protozoa (*17*), and filamentous fungi (*18*). An amphipathic α-helix structure is believed to be an important feature of these membrane-permeating peptides. Indeed, modeling the sequences of these peptides as idealized helices reveals their highly amphipathic nature, with hydrophobic residues on one face of the helix and polar or charged residues on the opposite face. Secondary structure prediction methods and CD spectroscopy have also shown that these peptides contain 45−90% helix in structure-promoting solvents. However, the helical structure of dermaseptins when bound to membranes has never been determined. Contrary to prediction methods and CD experiments, recent NMR studies showed that Drs S3 does not adopt an α-helical structure in TFE/water but has several turn-like regions along the polypeptide chain (*19*). Drs S4

* To whom correspondence should be addressed. Phone: 33 1 44 27 69 52. Fax: 33 1 44 27 59 94. E-mail: pnicolas@ccr.jussieu.fr.

[‡] Université Pierre et Marie Curie.

[§] Institut Jacques Monod.

[1] Abbreviations: CD, circular dichroism; CMC, critical micellar concentration; CSD, chemical shift deviation; Drs B2, dermaseptin B2; FTIR, Fourier transform infrared; ATR-FTIR, attenuated total reflection−FTIR; HSQC heteronuclear single-quantum correlation; NMR, nuclear magnetic resonance; NOE, nuclear Overhauser effect; NOESY, NOE spectroscopy; SDS, sodium dodecyl sulfate; TFA, trifluoroacetic acid; TFE, trifluoroethanol; TOCSY, total correlation spectroscopy.

10.1021/bi034401d CCC: $25.00
Published on Web 08/07/2003

was found to be highly aggregated, which prevented NMR analysis (*20*, *21*).

Drs B2 from *Phyllomedusa bicolor* is the most abundant member of the Drs B family and has the broadest active spectrum (*22*) but no hemolytic activity. It has the sequence GLWSK IKEVG KEAAK AAAKA AGKAA LGAVS EAV-NH_2. This 33-residue peptide has a molecular mass of 3180 Da with a tryptophan (Trp) at position 3 and six lysines (Lys) regularly spaced along the sequence. We have now investigated the secondary and tertiary structures of Drs B2 in membrane-mimetic environments and in TFE/water mixtures using CD, FTIR, fluorescence, and NMR spectroscopy in combination with molecular dynamics calculations. Our structural investigations revealed that Drs B2 has a helical propensity but adopts different structures in SDS and TFE/water mixtures. The N-terminal region of Drs B2 has a versatile structure and undergoes chemical shift heterogeneity at high peptide concentration in SDS. These structural features are discussed with respect to the interaction of the peptide with membranes.

EXPERIMENTAL PROCEDURES

Chemicals. 9-Fluorenylmethoxycarbonyl (Fmoc) protected L-amino acids and the peptide amide linker polyethylene glycol polystyrene-graft copolymer support (PAL-PEG-PS resin, substituted at 0.18 mequiv/g) were from Perseptive Biosystems. 5-Doxylstearic acid was from Sigma.

Solid-Phase Peptide Synthesis. Drs B2 was prepared by stepwise solid-phase synthesis using Fmoc polyamide active ester chemistry on a 9050 Pep Synthesizer Milli Gen. PAL-PEG-PS resin was used for carboxamidation of the C-terminal residue. Lysine and tryptophan side chains were protected with *tert*-butyloxycarbonyl (*t*-Boc), those of glutamic acid with *O*-*tert*-butyl ester (O*t*Bu), and those of serine with *O*-*tert*-butyl ether (*t*Bu). Synthesis was carried out using a triple-coupling protocol. N^{α}-Fmoc amino acids (4.4 molar excess) were coupled with 0.23 M diisopropylcarbodiimide for 30−60 min in a mixture of dimethylformamide and dichloromethane (60:40 v/v). Acylation was checked after each coupling step by the Kaiser test. Peptidyl resins were cleaved and side chains deprotected using 40 mg of peptidyl resin in 15 mL of a mixture composed of TFA (95%), triisopropylsilane (2.5%), and water (2.5%) for 2 h at room temperature. The resin was removed by filtering and the crude peptide precipitated with ether at 20 °C. It was then recovered by centrifugation at 5000*g* for 10 min, washed three times with cold ether, dried under nitrogen, dissolved in 10% acetic acid, and lyophilized. The crude Drs B2 was purified by preparative HPLC on a C18 reverse-phase column (N5C18-25M, Interchrom) eluted at 4 mL/min with a 40−60% linear gradient of acetonitrile in 0.07% TFA in water. The homogeneity of the synthetic peptide was assessed by analytical HPLC on a Lichrosorb C18 column (5 μm, 4.6 mm × 250 mm) eluted at 0.75 mL/min with a linear gradient of acetonitrile/0.07% TFA in 0.1% TFA acid/water. Peptide was detected by monitoring at 280 nm. Its identity was checked by MALDI-TOF mass spectrometry.

The two truncated derivatives with the sequences GL-WSKIKEVGK-NH_2 (Drs B2-[1−11]) and GKEAAKAAA-KAAGKAALGAVSEAV-NH_2 (Drs B2-[10−33]) were purchased from Neosystem (Strasbourg, France).

Measurement of Peptide Concentration. Drs B2 concentration was determined by measuring the absorbance at 280 nm (using a theoretical ϵ of 5600 $M^{-1}\cdot cm^{-1}$).

Circular Dichroism. CD spectra were recorded on a Jobin-Yvon Mark VI spectrometer interfaced to a PC microprocessor with DC6 software. The instrument outputs were calibrated with *d*(+)-10-camphorsulfonic acid (*23*). Spectra were measured at 25 °C over 190−260 nm, with a scan speed of 20 nm/min, a bandwidth of 1 nm, and a 1 mm path-length cell. Typically, five scans were accumulated and averaged. All dichroic spectra were corrected by subtracting the background obtained for each peptide-free mixture. The α-helix content was estimated from $\Delta\epsilon$ ($M^{-1}\cdot cm^{-1}$) at 222 nm, as described previously (*24*). The effects of SDS concentrations from 1 μM to 30 mM in aqueous solution and TFE concentrations from 10% to 80% (v/v) in aqueous solution were investigated with a Drs B2 concentration of 30 μM. Effects of various peptide concentrations from 30 to 250 μM were tested in 10 mM SDS.

FTIR Measurements. The trifluoroacetate counterions, which are strongly associated with the peptide, were replaced with chloride ions by lyophilizing the Drs B2 twice in 80 mM HCl before preparing the FTIR samples (*25*). Drs B2 was dissolved (2 mM) in a solution of 80 mM SDS in D_2O or in TFE/D_2O (20:80 v/v). Spectra were obtained at room temperature in dried air with a resolution of 4 cm^{-1} using a Perkin-Elmer Model 1720 FTIR spectrometer. Transmission spectra were obtained using an IR cell with CaF_2 windows and a 50 μm spacer. Second derivative analyses revealed that the 1600−1700 cm^{-1} amide I′ region involved five to six overlapping component bands representing different states of hydration and specific peptide secondary structures. The relative abundance of each structure was obtained by iterative least-squares fitting of the amplitude of each identified component band to the experimental amide I′ absorption band. Curves were fitted using the Origin 6.0 program for optimizing the amplitudes, band positions, half-width, and composition of the individual bands of a sum of Gaussian/Lorentzian profiles.

Fluorescence. Emission spectra were recorded on a Perkin-Elmer LS 50B spectrofluorometer linked to a PC microprocessor with Spectro Winlab software. The excitation wavelength was 280 nm, and the excitation and emission slit widths were 5 and 10 nm, respectively. Emission spectra were acquired in the 300−360 nm range at 1 nm increments with a scan speed of 20 nm/min at 25 °C. The Drs B2 concentration in water was 0.3 μM, and the SDS concentration varied from 1 μM to 100 mM. Tryptophan fluorescence was determined by subtracting spectra without peptide using Origin 6.0 software.

NMR Spectroscopy. All NMR samples were prepared in H_2O/D_2O (90:10) containing 80 mM SDS-d_{25} or in TFE-d_3/H_2O/D_2O (20:72:8 v/v); the Drs B2 concentration varied from 0.4 to 2 mM. Sodium trimethylsilylpropionate was used as an internal reference for chemical shift calibration. NMR spectra were recorded on Bruker Avance spectrometers operating at a ^1H frequency of 500 MHz and were processed with Bruker XWINNMR software. One-dimensional spectra were acquired over 16K data points using a spectral width of 6000 Hz. Solvent resonance was suppressed by presaturation during the relaxation delay (1.5 s) or with a WATERGATE sequence using pulsed field gradients (*26*).

Two-dimensional TOCSY (*27*) and NOESY (*28*) experiments were acquired in phase-sensitive mode using time-proportional phase incrementation (*29*), with the transmitter set on the solvent signal. The mixing times were 20−80 ms in TOCSY experiments and 100−250 ms in NOESY experiments. Two-dimensional data were usually collected with 400−600 t_1 increments and 2048 data points in t_2, over a spectral width of 6000 Hz in both dimensions. The time domain data were multiplied by a $\pi/3$-shifted square sine-bell function and zero-filled prior to Fourier transformation in t_2 and t_1. Baseline distortions were corrected with a fifth-order polynomial function. $^1H-^{13}C$ HSQC experiments were recorded using gradient pulses for coherence selection (*30*). The resonance assignments are listed in the tables in Supporting Information. The chemical shift deviations of HN, H^α, and C^α were calculated using random coil values reported in water (*31*).

NMR samples containing 0.3 mM Drs B2 in 80 mM SDS solution in H_2O/D_2O (90:10) were titrated with paramagnetic agents. $MnCl_2$ was dissolved in H_2O and added to the sample to obtain concentrations of 0.1−1.2 mM. 5-Doxylstearic acid was dissolved in CD_3OD and added to the sample to obtain concentrations of 1−2 mM. Two-dimensional TOCSY experiments were recorded at 45 °C with an isotropic mixing time of 40 ms.

Structure Calculation. Interproton distance restraints were derived from NOESY experiments recorded at 45 °C in SDS (100, 150, and 200 ms mixing times) and 15 °C in TFE (200 and 250 ms mixing times). The NOESY cross-peak intensities were converted to distance ranges of 0.18−0.28, 0.18−0.38, and 0.18−0.50 nm, corresponding to strong, medium, and weak NOEs. Different sets of distance restraints were used for the calculations in SDS. Pseudoatoms were introduced for distances involving methyl protons and unresolved methylene protons, and upper limits were corrected appropriately (*32*). The ϕ torsion angle was restrained to negative values for non-glycine residues which showed no strong intraresidual $d_{\alpha N}$ NOEs. The ψ torsion angle was restrained between −90° and 30° for residues having negative H^α CSDs below −0.1 ppm and C^α CSDs higher than 1 ppm. Structures were calculated using the AMBER force field (*33*) and InsightII version 98/Discover programs (Accelrys, San Diego, CA) running on SGI O2 R10000 workstations. Initial extended structures were submitted to 15 ps simulated annealing at 1000 K, during which the force constants of the distance and dihedral restraint terms were gradually increased. The nonbond interaction, defined by a simple quartic repulsive potential, was slowly increased during the next 10 ps (*34*). Finally, the structures were cooled from 1000 to 0 K over 25 ps. The structures were then minimized by steepest descent and conjugate gradient algorithms, using a Lennard-Jones potential for the van der Waals interaction and a distance-dependent dielectric screening of 4*r* for the electrostatic term.

Antimicrobial Assays. The antimicrobial activity was monitored by incubating 10 μL of each peptide (Drs B2-[1−11], Drs B2-[10−33], and Drs B2-[1−33], 0.2−100 μM) with an inoculum (100 μL/well, absorbance at 630 nm of 0.001) from overnight cultures of two Gram-positive (*Staphylococcus aureus, Bacillus megaterium*) or three Gram-negative (*Escherichia coli* 363, *Salmonella typhimurium, Enterobacter cloacae*) bacteria. The 96-well microtitration plates (Nunc F96) were incubated at 37 °C overnight, and the absorbance at 630 nm was measured by an ELISA reader (*35*). Minimal inhibitory concentrations (MICs) were defined as the dose at which growth was completely inhibited. Control incubations were carried out with 10 μL of formaldehyde to monitor the assay.

RESULTS

Secondary Structure of Dermaseptin B2 Inferred from CD Spectroscopy. Preliminary indications of the peptide secondary structure were obtained by CD measurements in water, in SDS solutions (Figure 1A), and in TFE/water mixtures (Figure 1B). The CD spectrum of Drs B2 (30 μM) in aqueous solution has a single negative band at 198 nm, typical of a peptide in random coil conformation (dotted line in Figure 1). The CD spectra for Drs B2 in low concentrations of SDS ($\leq$0.1 mM) show a broad minimum around 217 nm, suggesting the presence of some β-structure and/or turns. In contrast, the CD spectra at SDS concentrations near and above the CMC of SDS in water (5 mM; vide infra) indicate an enhanced helical content, with minima at 208 and 222 nm. The helix content increased with the SDS concentration until the Drs B2 was 55% helical (inset b, Figure 1A). The SDS-dependent folding of the peptide was complete at ~6 mM SDS, a concentration slightly above the CMC of SDS, indicating saturation of the peptide with the detergent. This SDS concentration roughly corresponds to a molar ratio of peptide/SDS micelles of 0.3:1, assuming 62 molecules of SDS per micelle (*36*). It seems unlikely that the structure is influenced by peptide−peptide interactions at this ratio. Thus, the peptide conformation changes that occur in the presence of SDS micelles are caused primarily by micelle binding. The spectra recorded in 10 mM SDS at SDS/peptide ratios of 40 to 320 (corresponding to peptide/SDS micelle ratios of 1.6 to 0.2) were also essentially identical (55 $\pm$ 2% helical content) (inset a, Figure 1A).

The CD spectra in TFE are characteristic of an α-helical conformation. The isodichroic point observed at 203 nm, together with variations of R1 and R2 ratios as a function of TFE concentration (*37*) indicate a strong cooperative transition from random coil to α-helix (Figure 1B). The helical content increased with the TFE concentration up to ~60% (v/v), corresponding to an α-helical content of 45%.

Secondary Structure of Dermaseptin B2 As Examined by FTIR Spectroscopy. The amide I′ spectra of 2 mM Drs B2 in D_2O (dotted line), in 80 mM SDS/D_2O (thick line), and in 20% TFE/D_2O (thin line) are shown in Figure 2A. The peptide carbonyl assignments of the various amide I′ components identified from second derivative spectra (Figure 2B,C) and the relative areas of each peak are summarized in Table 1. The maximum absorbance of the amide I′ band is at 1645 cm^{-1} in D_2O buffer and is shifted to 1647 cm^{-1} with SDS and 1643 cm^{-1} with TFE, suggesting structural changes. The IR analysis of Drs B2 between 1600 and 1700 cm^{-1} shows only five amide I′ component bands in SDS compared to six bands in 20% TFE/D_2O. The major band component, centered at 1656 cm^{-1} in both SDS and TFE, is attributable to an α-helical conformation (*5*, *38*). It involves about 58% of the total amide I′ area with 80 mM SDS and 27% with 20% TFE. These results correlate well with the CD analysis presented above. The amide I′ spectral compo-

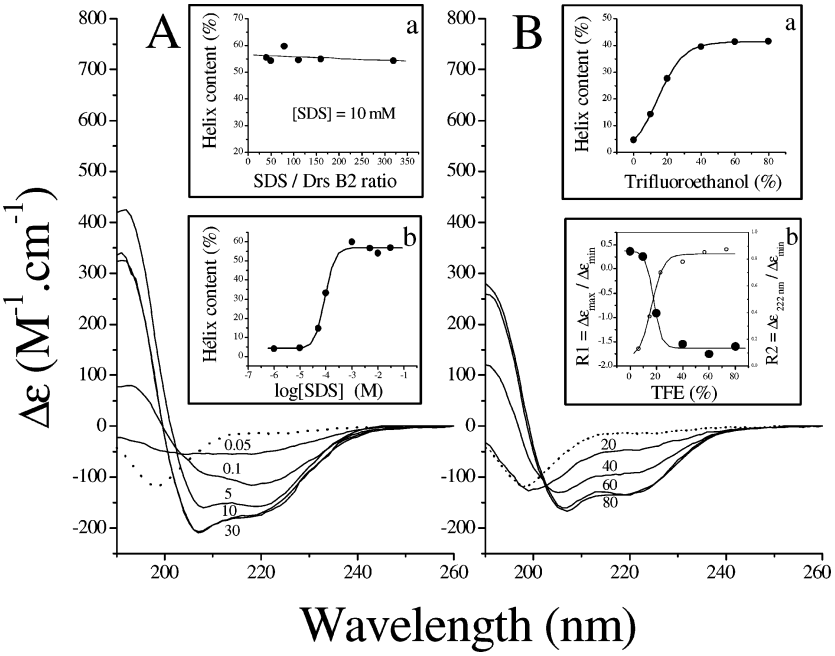

FIGURE 1: Far-UV CD spectra of dermaseptin B2 (30 μM) in aqueous solution (dotted line), in micellar and nonmicellar SDS (A), and in TFE (B). Numbers indicate the millimolar concentration of SDS (A) and the concentration of TFE in percent (v/v) (B). Inset a in (A) indicates the helix content as a function of SDS/Drs B2 ratio, with a fixed SDS concentration of 10 mM. Inset b in (A) shows the helix content versus increasing concentrations of SDS. The insets of (B) show the helix content (a) and the R1 and R2 ratios (*37*) (b) versus increasing concentrations of TFE. R1 (ratio between the intensity of the maximum between 190 and 195 nm and the intensity of the minimum between 195 and 210 nm) is ≤ -2 for highly helical peptides (>0 for a random coil peptide), while R2 (ratio between the intensity of the minimum near 222 nm and the intensity of the minimum between 195 and 210 nm) approaches $+1$ (0 for a random coil peptide).

nents between 1633 and 1646 cm^{-1} were attributed to random coil structures involving peptide carbonyls directly solvated by water, with probably one water molecule per carbonyl (*39*, *40*). The amide I′ contributions at 1670 and 1680 cm^{-1} also show the presence of weakly solvated peptide carbonyls (by TFE) and some that are not at all solvated. The occurrence of peptide carbonyls protected from water contacts implies the formation of local bends in the Drs B2 backbone (*6*, *25*). Obviously, the extent of both contributions decreased greatly when SDS was used instead of TFE (Table 1). We conclude that the helicity promoted by SDS is necessarily made at the expense of both hydrated (random) and unsolvated or weakly solvated domains (bent). The bent domain should involve more hydrophobic than polar side chains, while hydrated segments should have more polar than nonpolar side chains. This is in complete agreement with the amphipathicity of the promoted helical domain by SDS−peptide contacts as emerging from the NMR analysis of the same samples (see below). Most authors correlate amide I′ absorbance in this wavenumber range with H-bonded extended polypeptide strands forming β-sheet-like structures. Only a few have noticed that highly solvated single peptide groups, as in *N*-methylacetamide, also give rise to amide I′ absorbance in this spectral range. The low amide I′ wavenumber was attributed to the bonding of the amide carbonyl by two water molecules [C═O···$(D_2O)_2$]. While such complex formation may not be current in highly folded protein, it could be more accessible in short, very flexible peptide strands. Consequently, the infrared absorbances detected in the 1610−1646 cm^{-1} range in the presence of both SDS and TFE mean that about one-third of the Drs B2 backbone remains tightly bound to water molecules.

Monitoring the Binding of Dermaseptin B2 by Light Scattering and Fluorescence. The variations of light scattering intensity at 310 nm as a function of SDS concentration were recorded in the absence or presence of 0.3 μM Drs B2 (Figure 3A). The light scattering intensity remained relatively constant up to a SDS concentration of $\sim$2 mM in the absence of peptide (open circles). The sharp increase in intensity above this concentration corresponds to micelle formation that begins near the CMC. A CMC of 5 mM for SDS in water was calculated from the breakpoint determined by linear least-squares analysis of the two segments of the biphasic curve. A multiphasic curve was obtained when peptide was added (Figure 3A, black circle). The measured intensity remained constant up to a SDS concentration of $\sim$5 μM and then increased until a plateau was reached at a SDS concentration of $\sim$20 μM. Adding SDS above this concentration gave the classical value of CMC (5 mM) for SDS in water. This implies that a relatively large complex formed at 20 μM SDS. This might suggest that Drs B2 is bound to a SDS micelle at 20 μM SDS, a concentration that corresponds to a peptide/SDS ratio of $\sim$1:60, sufficient to accommodate one peptide per micelle. However, this would require the SDS micelles to form well below the CMC in the absence of peptide. On the other hand, the CD data for Drs B2 illustrate that SDS increased the helical structure of the peptide and that Drs B2 reached its maximum helical content slightly above the CMC (inset b, Figure 1B). While a consensus has not yet emerged as to what type of complex forms between cationic amphipathic peptides and SDS below the CMC, the formation of a small mixed micelle in which the anionic groups of SDS bind to the cationic groups of

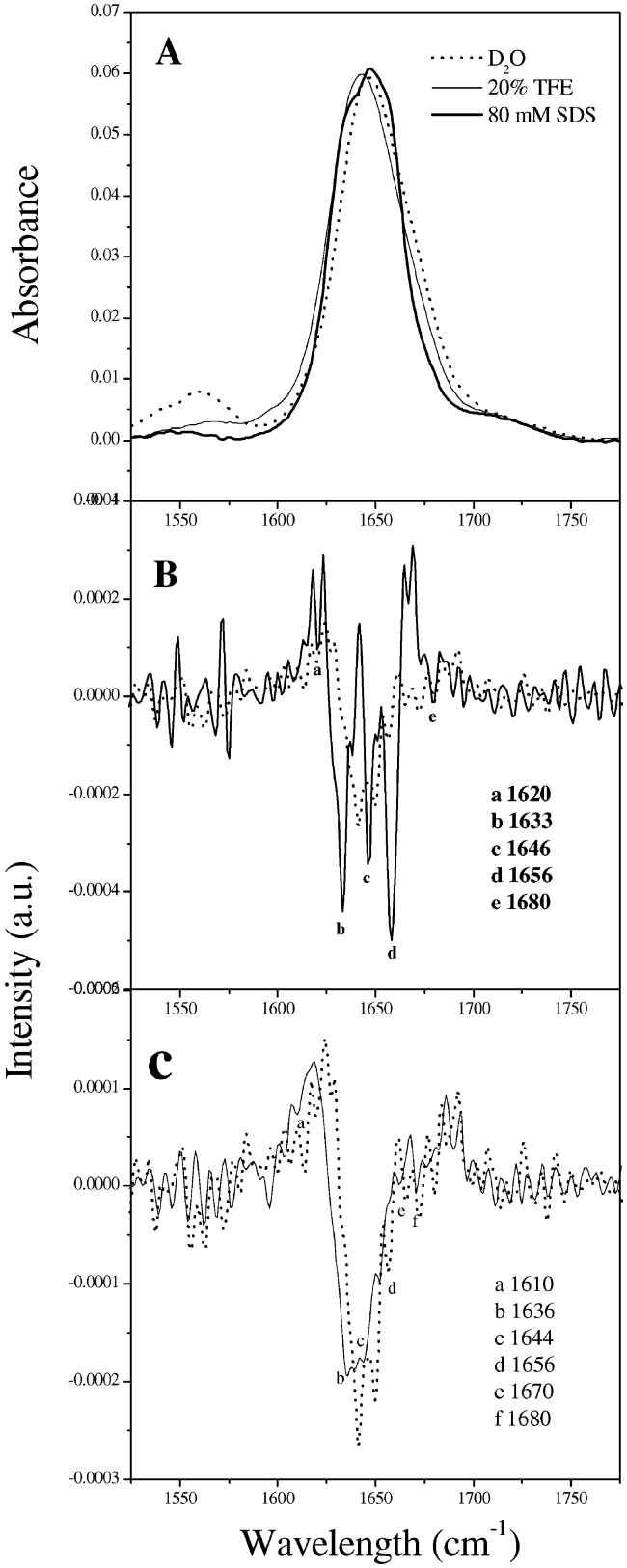

FIGURE 2: FTIR absorption spectra of dermaseptin B2. (A) Amide vibration domain of Drs B2 (2 mM) in D_2O (dashed line), 80 mM SDS (thick line), or 20% TFE (thin line). (B and C) Second derivatives of the amide I′ domain (1600−1700 cm^{-1}) in 80 mM SDS and 20% TFE; the second derivatives obtained in D_2O are shown with dashed lines.

the peptide while additional SDS molecules cluster around the extended peptide chain by hydrophobic forces could explain the data.

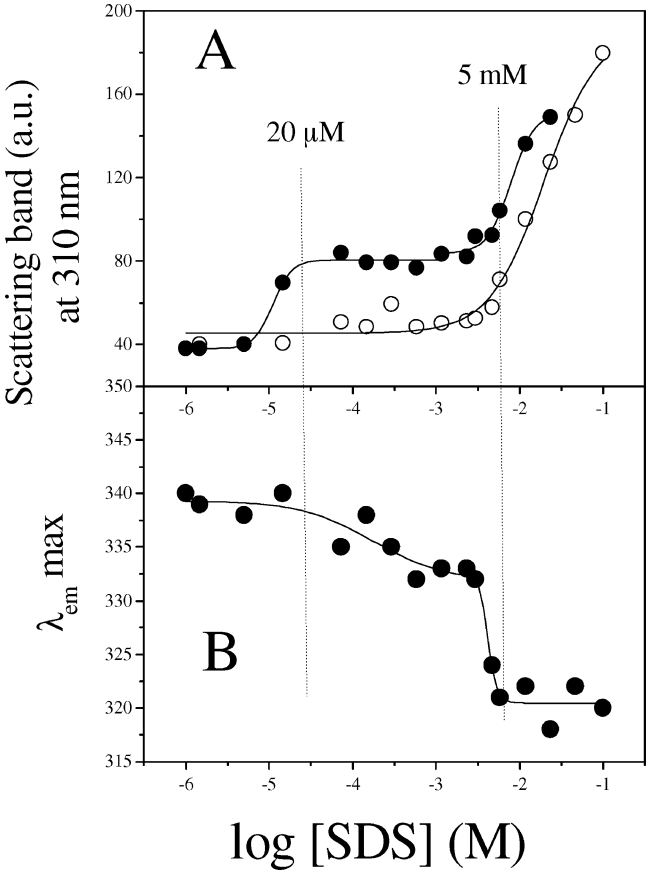

FIGURE 3: Fluorescence of dermaseptin B2 in SDS. (A) Intensity of the scattering band at 310 nm in the absence (open circles) or presence of 0.3 μM Drs B2 (black circles). (B) Emission maximum of tryptophan as a function of increasing concentrations of SDS (1 μM to 100 mM).

Table 1: Positions and Peptide Carbonyl Assignments of Individual Bands Resolved in the Amide I′ Domain of FTIR Spectra Obtained for 2 mM Drs B2 in D_2O with 80 mM SDS or 20% TFE

sample conditions	cm^{-1}	relative area (%)	estimated residue no.	peptide carbonyl assignment
80 mM SDS	1620	2	1	strongly H-bonded (β-sheet)
	1633 + 1646	24 + 16	13	hydrated (random)
	1656	58	19	α-helix
	1680	0.5	0	not solvated (bent or turn)
20% TFE	1610	4	1	strongly H-bonded (β-sheet)
	1636 + 1644	39 + 17	19	hydrated (random)
	1656	27	9	α-helix
	1670	6	2	weakly solvated (turn)
	1680	7	2	not solvated (bent or turn)

The interaction of Drs B2 (0.3 μM) with SDS was also followed by exploiting the intrinsic fluorescence of the Trp3 residue. We measured the relative intensity and maximum emission wavelength of tryptophan as a function of SDS concentration (Figure 3B). The fluorescence maximum of Drs B2 is at 340 nm in aqueous buffer (result not shown). The interaction of Drs B2 with SDS for peptide/SDS ratios of 30 to 1:3000 resulted in a blue shift of the emission maximum of about 5 nm without any noticeable change in the fluorescence intensity. This shift toward a shorter

wavelength paralleled the increase in light scattering intensity that was observed between 5 and 20 μM SDS. This small blue shift is similar to those reported for peptides having an indole group near a lipid−water interface (*41*) and that do not penetrate into the hydrophobic phase whatever the type of aggregate. In contrast, there was a much larger blue shift (20 nm) and enhanced quantum yield (up to 60%) at the SDS CMC. This suggests that the tryptophan of the peptide is selectively inserted into the acyl chain region of the SDS micelles (*42*).

NMR Spectroscopy of Drs B2 in Micellar SDS. NMR spectra of Drs B2 were recorded in 80 mM SDS in water, i.e., at a SDS concentration above the CMC. A high temperature (45 °C) was used because of broad resonance line widths. Surprisingly, the NMR spectra for 2 mM peptide in 80 mM SDS showed great overlaps and complexity, with more spin systems than expected for a 33-residue peptide. Decreasing the peptide concentration to 0.4 mM led to a single species that could be completely assigned using standard 2D homonuclear NMR. The ^{13}C resonances of C$^{\alpha}$ carbons were also partially assigned from 2D ^{13}C−^{1}H HSQC spectra. The assignment of Drs B2 at low concentration (0.4 mM) is listed in Table S1, available as Supporting Information.

The secondary structure of Drs B2 was analyzed using the chemical shifts of H$^{\alpha}$ and C$^{\alpha}$ resonances. Residues in helical conformations are known to show upfield shifts of H$^{\alpha}$ protons and downfield shifts of C$^{\alpha}$ carbons, while residues in extended conformations show the opposite trends (*43*). The chemical shift deviations (CSDs), calculated as the differences between observed chemical shifts and corresponding random coil values determined in water, are shown in Figure 4. Large upfield shifts of H$^{\alpha}$ and downfield shifts of C$^{\alpha}$ resonances were observed throughout the sequence of Drs B2 at low concentration (0.4 mM) in micellar SDS (Figure 4), indicating a high helical propensity for most residues. The sudden change of sign of the H$^{\alpha}$ CSD of Gly10 may indicate the presence of a turn or helix bend around this residue. Assuming a two-state equilibrium between random coil and helical conformations, the amount of helical structure in the peptide can be estimated from the set of CSD values. Thus, the overall percentage of α-helix is ∼60% (using an average CSD in helices of −0.39 ppm for H$^{\alpha}$ and 2.6 ppm for C$^{\alpha}$ (*44*)), which agrees with the CD and FTIR analysis.

The magnitude and pattern of interresidue nuclear Overhauser effects (NOEs) also give a qualitative indication of the secondary structure of Drs B2 (*45*). The diagram of sequential and medium-range connectivities obtained from NOESY experiments is available as Supporting Information (Figure S1). NOE correlations characteristic of α-helical conformation were observed throughout the peptide chain, including strong $d_{NN}(i, i + 1)$ and medium $d_{\alpha N}(i, i + 1)$ sequential connectivities, together with numerous $d_{\alpha N}(i, i + 3)$, $d_{\alpha\beta}(i, i + 3)$, and $d_{\alpha N}(i, i + 4)$ medium-range NOE connectivities.

Interestingly, periodic variations in the H$^{\alpha}$ and C$^{\alpha}$ CSDs were observed in segment 11−26 (Figure 4). The H$^{\alpha}$ protons of Lys residues at positions 11, 15, 19, and 23 all show large upfield shifts, while the H$^{\alpha}$ protons of the Ala residues at positions 13, 17, 21, and 24 show very weak upfield shifts. A similar periodicity was also detected for C$^{\alpha}$ CSDs. Moreover, amide protons exhibit a periodic change of sign of their CSDs. The HN protons of residues 13, 18, 22, 25, and 29 show large downfield shifts, whereas those of residues 16, 20, 24, 28, and 31 show upfield shifts. The CSD periodicity observed in SDS is consistent with the formation of an amphipathic helix with different environments of the polar face and the nonpolar face.

Reexamination of the 2 mM peptide sample and comparison with the assigned spectra at a lower Drs B2 concentration enabled us to partially assign residues 1−13 and 21−33 of Drs B2. Resonance overlap in the spectra prevented unambiguous assignments of residues 14−20. Indeed, assignment was hampered by the succession of Ala residues in this segment and broader resonances. Furthermore, the spectra recorded for 2 mM Drs B2 in 80 mM SDS showed the presence of chemical shift heterogeneity. The HN−H$^{\alpha}$ region of a 2D TOCSY experiment (Figure 5) shows three spin systems for Leu2, Trp3, Ile6, and Val9 and two spin systems for Ser4, Lys7, and Gly10, whereas a single spin system is observed for residues 21−33. The partial ^{1}H assignments of the different forms of Drs B2 at high concentration (2 mM) are listed in Table S2, available as Supporting Information. The three forms observed at high peptide concentration are indicated by A, B, and C. Form C is the major species, while forms A and B are minor species at high peptide concentration. The chemical shift similarities indicate that form A is very similar or identical to the single species observed at low peptide concentration.

The observed chemical shift heterogeneity involves the backbone as well as side-chain protons of residues 1−10 of Drs B2. In particular, the HN$^{\epsilon 1}$ and H$^{\delta 1}$ side-chain protons of Trp3 display up to three peaks, depending on the peptide concentration. The signals of the HN$^{\epsilon 1}$ proton of Trp3 in the different forms A, B, and C are observed in the low-field region of the 1D spectrum (Figure 6). Three resonances are observed for 2 mM Drs B2 in 80 mM SDS, and they are still visible until the peptide concentration decreases to 0.4 mM. The intensities of each resonance show a clear dependence on peptide concentration. The progressive decrease in the intensities of forms B and C as the peptide concentration decreased points to an equilibrium between the various forms at high peptide concentration, which are in slow exchange on the ^{1}H NMR time scale. This equilibrium is shifted to the A state at low concentrations. Since the chemical shift heterogeneity involves residues 1−10, the three states have different N-terminal environments. The small variations in chemical shift of states A and B indicate that the environments in the two states remain quite similar. In contrast, the large variations in the HN (>0.5 ppm) and H$^{\alpha}$ chemical shifts of Leu2 and Gly10 in the A and C states reflect large differences in the environment of the 1−10 segment.

NMR Spectroscopy of Drs B2 in TFE. A single species was observed for 2 mM Drs B2 in TFE/water, 20:80 (v/v), at 15 °C. Complete ^{1}H assignments are listed in Table S3, available as Supporting Information. Drs B2 has a nearly continuous stretch of downfield C$^{\alpha}$ chemical shifts (Figure 4A) and upfield H$^{\alpha}$ chemical shifts (Figure 4B) along the whole sequence, interrupted around residues Gly10, Gly22, and Gly27 and at the C-terminus (31−33). However, only the N-terminal half exhibits strong upfield shifts of H$^{\alpha}$ protons (CSDs < −0.1 ppm), indicating that the helical

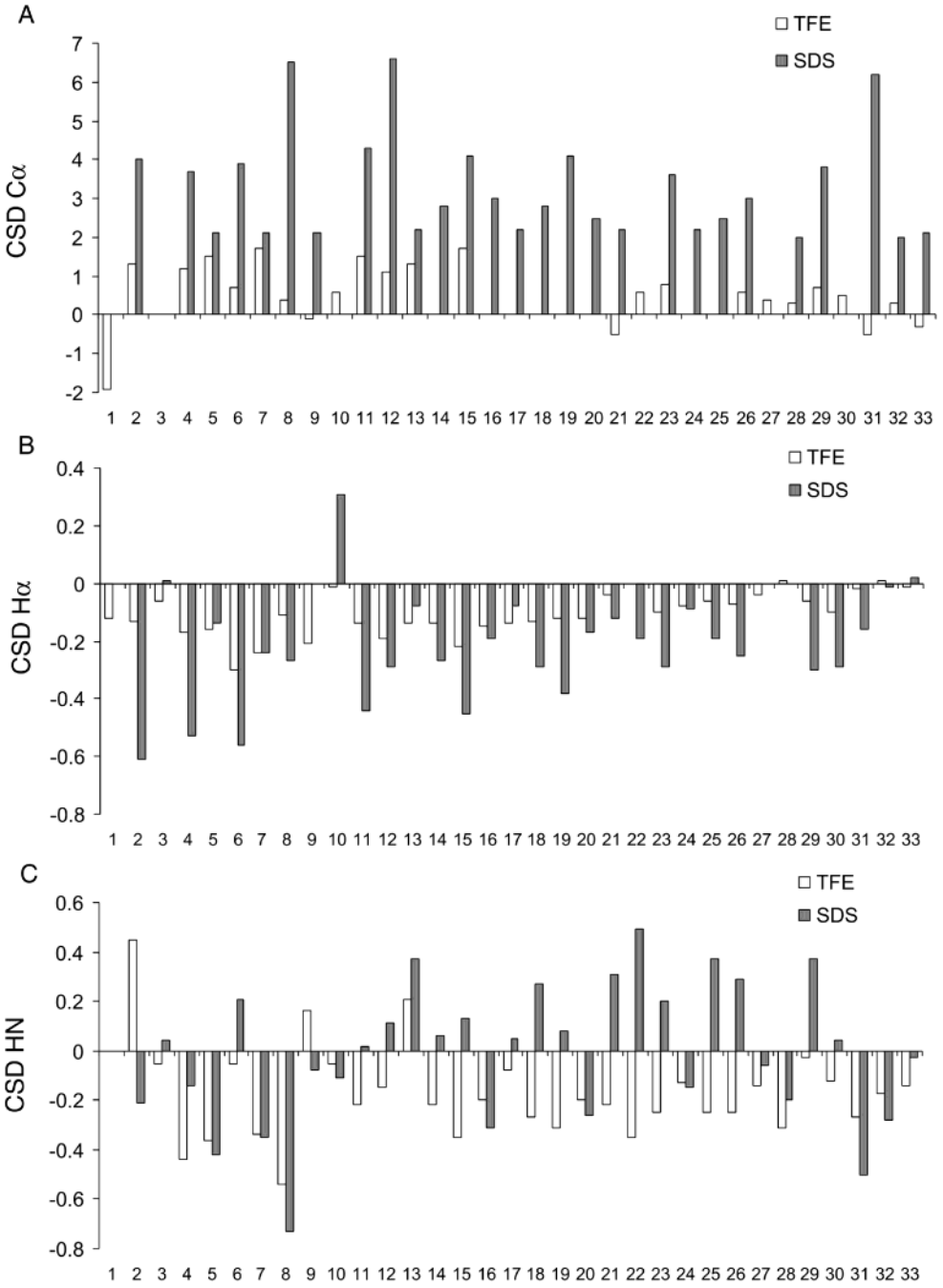

FIGURE 4: Chemical shift deviations of C^{α} carbons and H^{α} and HN protons of dermaseptin B2 in 80 mM SDS (0.4 mM Drs B2) or 20% TFE (2 mM Drs B2). The CSD values were calculated as the difference between observed chemical shifts and random coil chemical shifts.

propensity of Drs B2 in TFE is larger in the N-terminal segment. The amount of helical structure is estimated as 30% from CSDs. There are numerous $d_{\alpha N}(i, i + 3)$, $d_{\alpha\beta}(i, i + 3)$, and $d_{\alpha N}(i, i + 4)$ medium-range NOE connectivities along the sequence, further confirming the α-helical conformation of Drs B2.

Structure of Dermaseptin B2 in SDS and TFE. The structures of Drs B2 in 80 mM SDS and in 20% TFE were calculated by restrained molecular dynamics with Discover. The structure of Drs B2 at a concentration of 0.4 mM in SDS (Figure 7A) was calculated using a set of 182 distance restraints (including 43 medium- and long-range restraints). Drs B2 forms a well-defined amphipathic helix in SDS, extending from residue 11 to the C-terminus (backbone rmsd of 0.96 Å for residues 11−31). The calculations led to systematic distance violations in the N-terminal 3−8 segment, due to conflicting NOEs. Indeed, in addition to the medium-range NOEs typical of an α-helix, three long-range NOEs were observed between Leu2 and Glu8 that are not compatible with an α-helical conformation of this segment. These 2−8 NOE correlations might come from an alternative conformation in fast exchange on the NMR time scale with a more regular helical structure. We therefore did additional calculations with different sets of distance restraints for residues in the N-terminal segment, one corresponding to helical-type restraints and the other with the 2−8 restraints. The N-terminal segment adopts a better defined α-helical structure between residues 3 and 8 without the 2−8 restraints, which is connected to the long 11−33 helix by a loose structure around Val9 and Gly10 (data not shown). This is

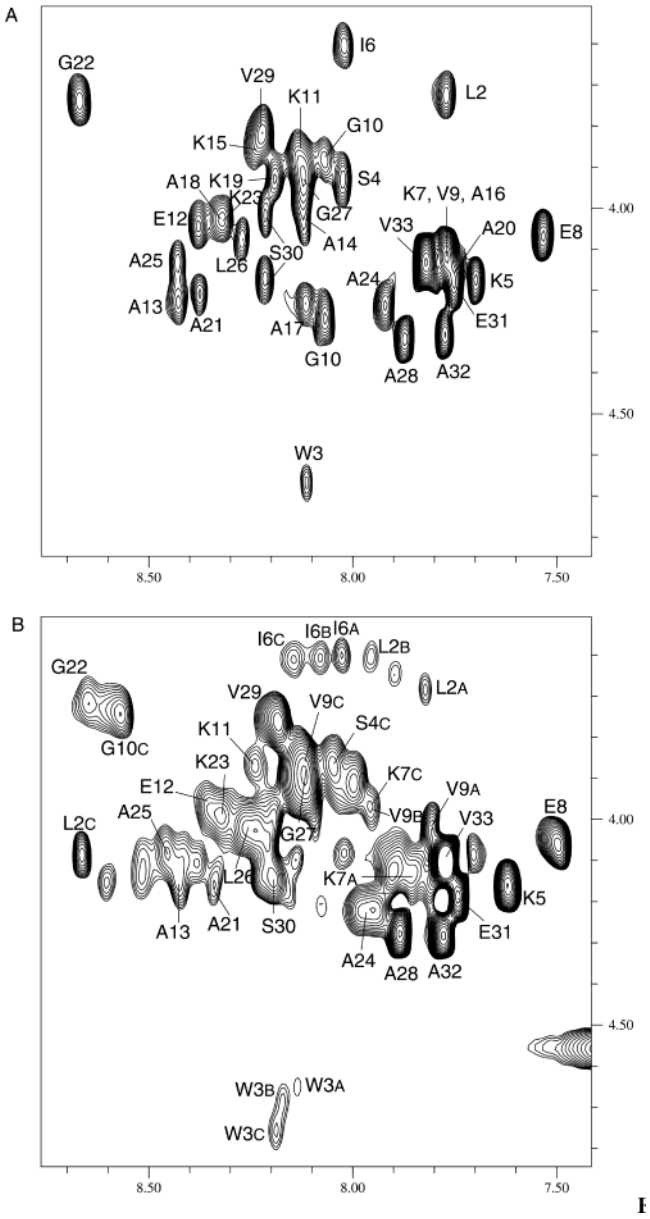

FIGURE 5: HN−H$^{\alpha}$ region of 2D TOCSY spectra of dermaseptin B2 in 80 mM SDS obtained at 0.4 mM (A) and 2 mM (B) peptide concentration. The assignments of the N-terminal region in the different forms at 2 mM are indicated by the letters A, B, and C.

in agreement with the change of the sign of the H$^{\alpha}$ CSD of Val9. The structures calculated with 2−8 distance restraints but without α-helical restraints in the N-terminal part are poorly defined (not shown). Two types of folds can be observed: a hairpin-like structure with the N-terminus and residue 8 close together or a loose helical structure.

We could not determine the structures of states B and C at higher concentration owing to incomplete assignments and few assigned NOEs. Although the central segment 14−20 could not be assigned, there are many unassigned HN−HN cross-peaks on NOESY spectra, indicating the presence of helical conformations in this region. The N-terminal segment 1−10 has NOEs typical of an α-helical structure in state C. In particular, the NOE correlations between Leu2 and Glu8 are not seen in state C.

The structures of Drs B2 in TFE, calculated from the analysis of 162 NOE cross-peaks (including 46 medium-range connectivities), are shown in Figure 7B. The structures

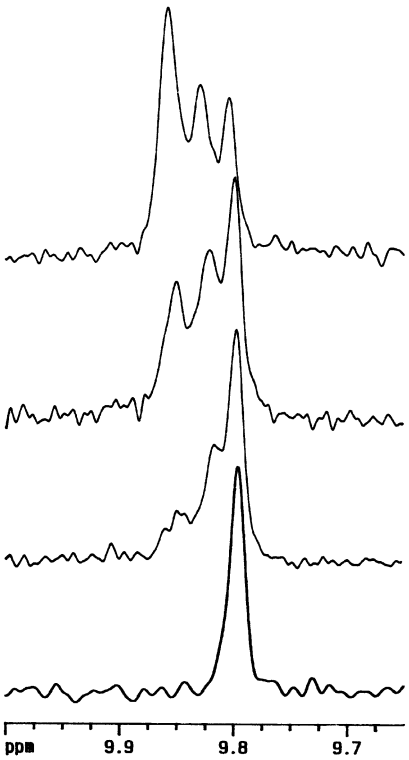

FIGURE 6: Low-field region of the 1D ^{1}H spectrum showing the HN$^{\epsilon 1}$ resonance of Trp3 of dermaseptin B2 in 80 mM SDS (500 MHz, 45 °C). The concentrations of Drs B2 are, from top to bottom, 2, 1.4, 1, and 0.4 mM. The titration was started from a sample of 2 mM Drs B2 in 80 mM SDS and was performed by diluting the peptide with 80 mM SDS.

have low energies and few restraint violations, with an average of four distance violations greater than 0.1 Å. The rmsd of backbone atoms (N, C$^{\alpha}$, C′) is very large (5.8 Å) but decreases to 1.1 Å when only residues 3−18 are taken into account. Segment 3−18 forms a well-defined helix which is slightly bent around Gly10. In contrast, the C-terminal segment (19−33) is more disordered, although there are short helices around residues 25 and 30 in several structures.

Positioning Experiments in SDS Micelles. The position of Drs B2 relative to SDS micelles was investigated using two paramagnetic probes, $MnCl_2$ and 5-doxylstearic acid. Mn^{2+} should cause the resonances of residues exposed to solvent to broaden, while 5-doxylstearic acid should cause the resonances for residues buried inside the micelle but close to the surface to broaden (*46*). The residual amplitudes of selected cross-peaks in TOCSY spectra after addition of paramagnetic agents are shown in Figure 8. Residues of Drs B2 were affected differently by the paramagnetic Mn^{2+} ions. The correlations from residues 30−32 in the C-terminus disappeared when $MnCl_2$ (0.1 mM) was first added. The correlations from residues 28, 29, and 33 disappeared at 0.2−0.3 mM $MnCl_2$, and the correlations from residues 8, 9, 12, 24, 25, and 27 were lost at 0.5−0.8 mM $MnCl_2$. Interestingly, the most severely affected residues are in the vicinity of three Glu residues (Glu31, Glu8, and Glu12). This could be due to an electrostatic interaction of the carboxylic group with Mn^{2+} ions. The sensitivity to paramagnetic Mn^{2+} for the three Glu residues is different (Glu12 < Glu8 < Glu31) and may reflect slight differences in accessibility. Most residues were broadened at higher concentrations of $MnCl_2$, but those in

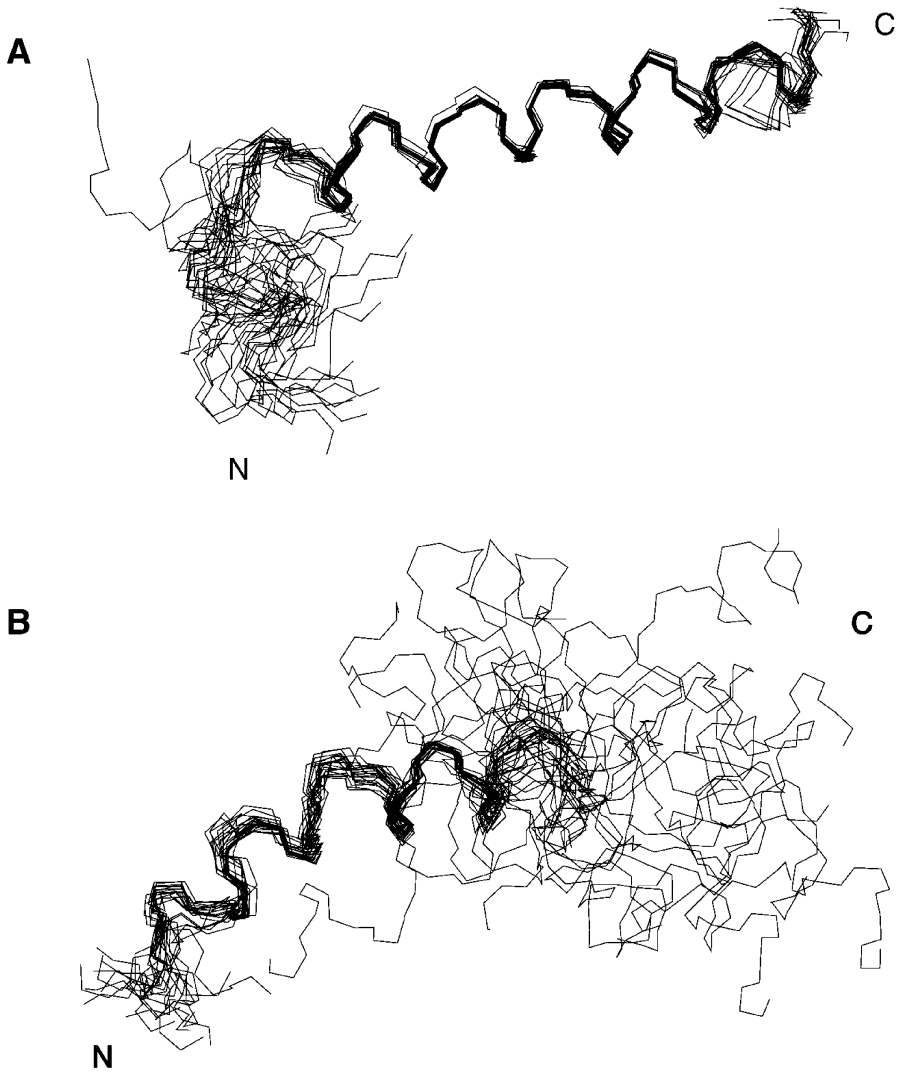

FIGURE 7: NMR structures of dermaseptin B2 in 80 mM SDS and 20% TFE. (A) Family of 20 structures obtained from NMR data collected for 0.4 mM Drs B2 in 80 mM SDS. Structures were superimposed by fitting the backbone atoms N, C^{α}, and C′ from residue 11 to residue 31. (B) Family of 20 structures obtained from the NMR data determined in 20% TFE with 2 mM Drs B2. Structures were superimposed by fitting the backbone atoms N, C^{α}, and C′ from residue 3 to residue 18.

the N-terminal (3−7) and in the central segment (13−23) were less affected. The addition of 5-doxylstearic acid mainly affected the resonances of the Trp3 side-chain proton, especially its $HN^{\epsilon 1}$ proton, which underwent considerable broadening (Figure 8B). The residual amplitudes of other cross-peaks were affected to similar extents. Ala21 and Ala25 were the most affected, since their cross-peaks disappeared when 3 mM 5-doxylstearic acid was added.

Antimicrobial Activity of Dermaseptin B2 and Truncated Derivatives. Two peptide derivatives, Drs B2-[1−11] and Drs B2-[10−33], were assayed against model microorganisms to evaluate the structural features responsible for the antimicrobial activity of Drs B2. These peptides encompass the N-terminal region and the C-terminal helix domain of the peptide in the micellar SDS environment, respectively. The susceptibility of various bacteria to Drs B2 and its derivatives was assessed by measuring the minimal inhibitory concentration (MIC) of the peptides against five strains of Gram-positive and Gram-negative bacteria (Table 2). Drs B2 was very active against all the microorganisms tested, with MICs of 0.5−6.25 μM. The N-terminally truncated analogue, Drs B2-[10−33], was inactive against these bacteria up to the highest concentration tested (100 μM). This indicates that the N-terminal region of Drs B2 is essential for bactericidal activity, at least against these microorganisms. The C-terminally truncated analogue Drs B2-[1−11] was much less active than the parent molecule against *B. megaterium, E. coli and E. cloacae* and was inactive against *S. aureus* and *S. typhimurium*. Therefore, both helical domains appear to be required for full antimicrobial activity.

DISCUSSION

One goal of this study was to compare the conformations adopted by Drs B2 in structure-promoting solvents (TFE/water mixtures) and in SDS used to mimic a membrane environment.

The results of CD, FTIR, and fluorescence light scattering indicate that Drs B2 undergoes complex solvent-induced structural transitions, depending on environmental conditions. Whereas Drs B2 assumes a predominantly random coil conformation in water, CD and FTIR investigations revealed that the peptide undergoes a simple random coil to α-helix transition in TFE/water. Drs B2 has no regular structure in

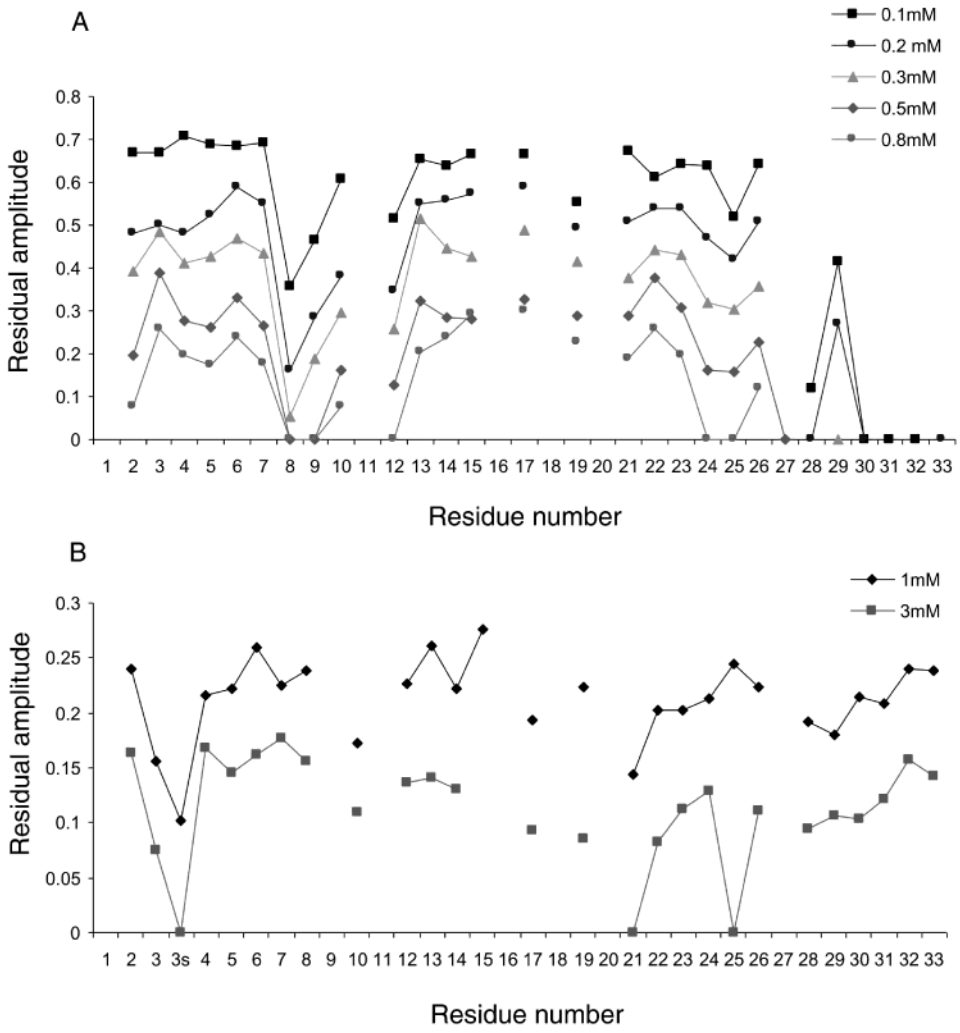

FIGURE 8: Remaining amplitudes of TOCSY cross-peaks of 0.4 mM Drs B2 in 80 mM SDS after addition of paramagnetic probes. (A) Titration with $MnCl_2$. (B) Titration with 5-doxylstearic acid. The remaining amplitudes were measured on resolved HN−H^{α} cross-peaks. The $H^{\epsilon 1}$−$H^{\delta 1}$ cross-peak was used for the Trp3 side chain (labeled 3s).

Table 2: Antibacterial Activity of Drs B2-[1−33], Drs B2-[1−11], and Drs B2-[10−33]

bacteria strain[a]	minimal inhibitory concn (μM)		
	Drs B2-[1−11]	Drs B2-[10−33]	Drs B2
firmicutes (Gram-positive eubacteria)			
S. aureus	R	R	6.25
B. megaterium	45%[b]	R	1.56
gracilicutes (Gram-negative eubacteria)			
E. coli 363	70%[b]	R	0.39
S. typhimurium	R	R	3.12
E. cloacae	30%[b]	R	5.00

[a] Strains (IBMC Strasbourg) were considered resistant (R) when their growth was not at all inhibited by peptide concentrations up to 100 μM. [b] Percentages correspond to maximal growth inhibition obtained at 100 μM.

solutions containing very low concentrations of SDS (<10 μM). Increasing the SDS concentration to 50 μM promotes the formation of a complex between the peptide and SDS monomers. The driving forces are probably the electrostatic interactions between the positive charges of the lysine side chains of Drs B2 and the negatively charged sulfate groups of the SDS molecules and the hydrophobic interactions between SDS acyl chains and the extended peptide chain. These interactions at SDS concentrations well below the CMC are not sufficient to cause Drs B2 to adopt a helical conformation. The peptide gave CD spectra somewhat reminiscent of extended structures, although it is difficult to separate the contributions of a variety of β-sheets, β-turns, and other structures. Others have shown that submicellar concentrations of SDS tend to induce extended conformations, while micellar concentrations lead to helical structures (*24*, *47*, *48*). The small contributions of β-structure and/or turns to the conformation equilibrium at low SDS concentrations may explain the lack of a clear isodichroic point in CD spectra (Figure 1A). A micellar SDS environment causes major conformational changes since the nonhelical structure is converted into an α-helical state with ∼55% helix content.

The helical conformation of Drs B2 in 80 mM SDS and 20% TFE, inferred by CD and FTIR data, was further examined by NMR spectroscopy combined with molecular dynamics calculations. In 20% TFE, Drs B2 adopts a well-defined α-helix between positions 3 and 18. Segment 19−33 has a weaker helical propensity and forms loose helical structures. The Gly residues at positions 22 and 27 may act as helix breakers that destabilize the helical structure in this C-terminal segment. The N-terminal helix is also slightly

deformed around Gly10, but medium-range NOE correlations around this residue suggest that the helix is not interrupted. In 80 mM SDS, NMR spectroscopy revealed that Drs B2 undergoes complex equilibria dependent upon peptide concentration (from 0.4 to 2 mM, corresponding to peptide/SDS ratios of 1:40 to 1:200). A single set of proton resonances was observed at low peptide concentration (0.4 mM), with a peptide/SDS micelle ratio of 0.3:1, which corresponds to a highly helical (60%) state. The proportion of α-helix is higher than in 20% TFE (27−30%). Comparison of the structures of Drs B2 in 20% TFE and in 80 mM SDS also shows that the peptide conformations in these media differ significantly. While the helical structure of Drs B2 extends from Trp3 to Ala18 and is followed by a more flexible, loosely defined helix segment in TFE/water, Drs B2 has a well-defined α-helix spanning residues 11−33. There is also a loose helical segment encompassing residues 3−8 that is separated from the well-defined helix by a small hinge region consisting of residues Val9 and Gly10. Helix 11−33 is totally amphipathic; that is, the apolar side chains (mostly Ala) are aligned on a portion of the helical cylinder, whereas the polar and charged residues (Lys) occupy the remaining surface. The orientation of the N-terminal segment relative to the helix of residues 11−33 is poorly defined owing to the hinge region 9−10.

The interaction of Drs B2 with SDS micelles can be inferred from the periodic variations of H^{α}, C^{α}, and HN CSDs in the segment 11−26. This periodicity of HN CSDs has also been observed for mastoporan and transportan (*49*) in micelles and bicelles. This behavior can be ascribed to the burying of the nonpolar face of the helix (formed by Ala residues) in the hydrophobic core of the SDS micelles. Periodic variations of H^{α} and HN proton chemical shifts have also been reported for amphipathic peptides that have a curved helical domain (*50*, *51*). Consequently, the CSD periodicity could also indicate that the 11−26 helix is curved, leading to shorter hydrogen bonds on the nonpolar, concave surface and longer hydrogen bonds on the hydrophilic, convex side. This curvature could allow the optimal amphipathic distribution of the amino acid side chains and hence adaptation of the helical structure to the curved surface of SDS micelles. Such helix curvature is not observed in the family of calculated structures. However, linear and curved helices exhibit only very little differences in their sequential and medium-range NOEs, and these are not likely to come out using qualitative categorization of NOE cross-peaks.

The position of Drs B2 relative to the SDS micelle surface was investigated using paramagnetic probes. Titration with Mn^{2+} indicates that segments 8−12 and 24−33 are accessible to the paramagnetic ion. The 5-doxyl spin-labeling experiments and fluorescence data show that residue Trp3 in the N-terminal segment of the peptide lies inside the SDS micelles. Since the paramagnetic group of 5-doxylstearic acid is close to the polar head, the side chain of Trp3 is buried inside the micelle but remains close to the surface. Thus, these results suggest that Drs B2 is mainly located at the interface between SDS micelles and water.

The N-terminal segment adopts helical conformations, but the conflicting NOE data could indicate conformations that are rapidly interconverting on the NMR time scale. The conformations might correspond to different states of interaction with SDS micelles. Alternatively, the correlations between Leu2 and Glu8 could be due to intermolecular NOEs. However, this is unlikely since these NOEs are observed only at low peptide concentrations.

The NMR spectra of Drs B2 showed the formation of two other species at higher peptide/SDS ratios. These forms are in slow exchange on the NMR time scale and have different sets of resonances in the N-terminal 1−10 segment. The NMR spectra of 2 mM Drs B2 in 20% TFE show only one set of resonances, demonstrating that the slow exchange is induced by interactions between Drs B2 and SDS micelles. The observed chemical exchange could reflect oligomerization of Drs B2, since it is observed at the highest peptide concentration (peptide/SDS micelle ratio of 1.3:1). The alternative states B and C may correspond to the association of at least two molecules of Drs B2 per SDS micelle. These two peptide molecules bound to the micelle surface must adopt nearly identical arrangements of their C-terminal parts, leading to a single set of resonances for the corresponding residues in all three forms. In contrast, they differ in the environment of their N-terminal segments. Such differences could be due to distinct modes of interaction with SDS micelles or from an asymmetrical arrangement of the N-terminal part in the postulated oligomeric forms. Although the structure of state C could not be determined, the differences in chemical shift affecting residues Leu2 and Gly10 and the absence of NOEs between Leu2 and Glu8 indicate that the conformation of its N-terminal segment is very different from that of state A. The most surprising result concerns the rate of exchange between the different states, which is slow on the NMR time scale. The exchange of free SDS molecules with SDS micelles is fast on the NMR time scale, which a priori implies the same exchange regime for any molecules interacting with SDS micelles. This finding emphasizes the strong associative and stabilizing properties of Drs B2 for negatively charged amphipathic detergent molecules.

The conformational versatility of the N-terminal segment led us to investigate its role in antimicrobial activity. The structure−activity study of truncated Drs B2 analogues shows that the N-terminal truncated analogue Drs B2-[10−33] is completely devoid of activity. Deleting the C-terminal peptide helix to give Drs B2-[1−11] drastically decreased the antibacterial potency (Table 2). This demonstrates that the N-terminal segment is necessary for antibacterial activity of Drs B2. However, the entire peptide length is required for full permeabilization potency.

Comparison with Other Antimicrobial Peptides. Many α-helical antimicrobial peptides, such as magainins (*52*, *53*), belong to the class L amphipathic helices (*54*). Class L helices possess a wide, bulky nonpolar face and a narrow hydrophilic face containing a number of cationic residues (preferentially lysine) that show bimodal clustering at the interfaces of the polar and nonpolar faces. The Drs B2 amphipathic helix differs significantly from class L helices. The positively charged polar face of Drs B2 subtends a radial angle of 180° perpendicular to the long axis of the helix, which is much greater than the average (100°) for class L helices. The lysine residues are randomly distributed along the perimeter of the polar face, and the hydrophobic face contains essentially small alanine residues. Despite great sequence similarities with Drs B2, Drs S3 and Drs S4 show very little or no helix content in TFE/water (*19*, *20*).

However, structure−function studies indicate that replacing Met4 and Asn20 by Lys in Drs S4 induces an α-helical structure from the N-terminus up to residue 13 (*20*). Since Drs B2 and [Lys4,20]Drs S4 have similar lengths and identical net positive charges, these observations indicate that a variety of parameters, including hydrophobicity, hydrophobic moment, bulk of the apolar face, and the angle subtended by the hydrophobic residues, have all crucial influences on the helix content and stability of dermaseptins.

CONCLUSION

A key finding of this study is that the structures of Drs B2 in TFE and in micellar SDS differ significantly. In particular, the N-terminal 1−11 segment, which was shown to be crucial for antibacterial activity, can adopt different conformations depending on the environment (TFE versus SDS, peptide/SDS ratios). This suggests that a negatively charged hydrocarbon−water interface is not essential for α-helix formation, but it is important for proper conformational adjustment to enable the peptide helix to interact optimally with the micelle surface. The electrostatic interactions between the positively charged lysine residues at the C-terminal domain of the peptide and the anionic SDS headgroups could drive primary binding and anchoring to the micelle surface. The conformational flexibility of the N-terminal segment and the Val9−Gly10 hinge region may facilitate the penetration of Trp3 into the SDS micelles.

ACKNOWLEDGMENT

We thank S. Noinville for FTIR technical assistance and M.-H. Baron for critically reading the FTIR part of the manuscript.

SUPPORTING INFORMATION AVAILABLE

Table S1, assignment of 0.4 mM dermaseptin B2 in 80 mM SDS (45 °C), Table S2, partial assignment of 2 mM dermaseptin B2 in 80 mM SDS (45 °C), Table S3, assignment of dermaseptin B2 in 20% TFE (15 °C), and Figure S1, summary of sequential and medium-range NOEs observed for 2 mM dermaseptin B2 in TFE (A) and 0.4 mM dermaseptin B2 in 80 mM SDS (B). This material is available free of charge via the Internet at http://pubs.acs.org.

REFERENCES

1. Simmaco, M., Mignogna, G., and Barra, D. (1998) *Biopolymers 47*, 435−450.
2. Shai, Y. (1999) *Biochim. Biophys. Acta 1462*, 55−70.
3. Sonnichsen, F. D., Van Eyk, J. E., Hodges, R. S., and Sykes, B. D. (1992) *Biochemistry 31*, 8790−8798.
4. Oren, Z., and Shai, Y. (2000) *Biochemistry 39*, 6103−6114.
5. Boncheva, M., and Vogel, H. (1997) *Biophys. J. 73*, 1056−1072.
6. Tatulian, S. A., Jones, L. R., Reddy, L. G., Stokes, D. L., and Tamm, L. K. (1995) *Biochemistry 34*, 4448−4456.
7. Ludtke, S. J., He, K., Heller, W. T., Harroun, T. A., Yang, L., and Huang, H. W. (1996) *Biochemistry 35*, 13723−13728.
8. Williams, R. W., Starman, R., Taylor, K. M., Gable, K., Beeler, T., Zasloff, M., and Covell, D. (1990) *Biochemistry 29*, 4490−4496.
9. Park, S., Park, S. H., Ahn, H. C., Kim, S., Kim, S. S., and Lee, B. J. (2001) *FEBS Lett. 507*, 95−100.
10. Fleury, Y., Dayem, M. A., Montagne, J. J., Chaboisseau, E., Le Caer, J. P., Nicolas, P., and Delfour, A. (1996) *J. Biol. Chem. 271*, 14421−14429.
11. Brand, G. D., Leite, J. R., Silva, L. P., Albuquerque, S., Prates, M. V., Azevedo, R. B., Carregaro, V., Da Silva, J. S., Sa, V. C., Brandao, R. A., and Bloch, C., Jr. (2002) *J. Biol. Chem. 277*, 49332−49340.
12. Charpentier, S., Amiche, M., Mester, J., Vouille, V., Le Caer, J. P., Nicolas, P., and Delfour, A. (1998) *J. Biol. Chem. 273*, 14690−14697.
13. Strahilevitz, J., Mor, A., Nicolas, P., and Shai, Y. (1994) *Biochemistry 33*, 10951−10960.
14. Nicolas, P., and Mor, A. (1995) *Annu. Rev. Microbiol. 49*, 277−304.
15. Daly, J. W., Caceres, J., Moni, R. W., Gusovsky, F., Moos, M., Jr., Seamon, K. B., Milton, K., and Myers, C. W. (1992) *Proc. Natl. Acad. Sci. U.S.A. 89*, 10960−10963.
16. Mor, A., Hani, K., and Nicolas, P. (1994) *J. Biol. Chem. 269*, 31635−31641.
17. Hernandez, C., Mor, A., Dagger, F., Nicolas, P., Hernandez, A., Benedetti, E. L., and Dunia, I. (1992) *Eur. J. Cell Biol. 59*, 414−424.
18. Mor, A., Nguyen, V. H., Delfour, A., Migliore-Samour, D., and Nicolas, P. (1991) *Biochemistry 30*, 8824−8830.
19. Shalev, D. E., Mor, A., and Kustanovich, I. (2002) *Biochemistry 41*, 7312−7317.
20. Kustanovich, I., Shalev, D. E., Mikhlin, M., Gaidukov, L., and Mor, A. (2002) *J. Biol. Chem. 277*, 16941−16951.
21. Feder, R., Dagan, A., and Mor, A. (2000) *J. Biol. Chem. 275*, 4230−4328.
22. Mor, A., Amiche, M., and Nicolas, P. (1994) *Biochemistry 33*, 6642−6650.
23. Chen, Y. H., Lo, T. B., and Yang, J. T. (1977) *Biochemistry 16*, 1826−1830.
24. Zhong, L., and Johnson, W. C., Jr. (1992) *Proc. Natl. Acad. Sci. U.S.A. 89*, 4462−4465.
25. Surewicz, W. K., Mantsch, H. H., and Chapman, D. (1993) *Biochemistry 32*, 389−394.
26. Piotto, M., Saudek, V., and Sklenar, V. (1992) *J. Biomol. NMR 2*, 661−665.
27. Bax, A., and Davis, D. G. (1985) *J. Magn. Reson. 65*, 355−360.
28. Kumar, A., Ernst, R. R., and Wüthrich, K. (1980) *Biochem. Biophys. Res. Commun. 95*, 1−6.
29. Marion, D., and Wüthrich, K. (1983) *Biochem. Biophys. Res. Commun. 113*, 967−974.
30. Schleucher, J., Schwendinger, M., Sattler, M., Schmidt, P., Schedletzky, O., Glaser, S. J., Sorensen, O. W., and Griesinger, C. (1994) *J. Biomol. NMR 4*, 301−306.
31. Wishart, D. S., Bigam, C. G., Holm, A., Hodges, R. S., and Sykes, B. D. (1995) *J. Biomol. NMR 5*, 67−81.
32. Wüthrich, K., Billeter, M., and Braun, W. (1983) *J. Mol. Biol. 169*, 949−961.
33. Weiner, S. J., Kollmann, P. A., Nguyen, D. T., and Case, D. A. (1986) *J. Comput. Chem. 7*, 230−252.
34. Nilges, M., Clore, G. M., and Gronenborn, A. M. (1988) *FEBS Lett. 229*, 317−324.
35. Casteels, P., Ampe, C., Jacobs, F., and Tempst, P. (1993) *J. Biol. Chem. 268*, 7044−7054.
36. Mysels (1959) *Introduction to colloid chemistry*, Interscience, New York.
37. Bruch, M. D., Dhingra, M. M., and Gierasch, L. M. (1991) *Proteins 10*, 130−139.
38. Goormaghtigh, E., Cabiaux, V., and Ruysschaert, J. (1994) *Subcellular biochemistry: physicochemical methods in the study of biomembranes*, Vol. 23, Plenum Press, New York.
39. De Lozé, C., Baron, M.-H., and Fillaux, F. (1978) *J. Chim. Phys. 75*, 631−649.
40. Wantyghem, J., Baron, M.-H., Picquart, M., and Lavialle, F. (1990) *Biochemistry 29*, 6600−6609.
41. De Kroon, A. I., Soekarjo, M. W., De Gier, J., and De Kruijff, B. (1990) *Biochemistry 29*, 8229−8240.
42. Li, S. C., and Deber, C. M. (1994) *Nat. Struct. Biol. 1*, 558.
43. Wishart, D. S., Sykes, B. D., and Richards, F. M. (1991) *J. Mol. Biol. 222*, 311−333.
44. Wishart, D. S., and Sykes, B. D. (1994) *Methods Enzymol. 239*, 363−392.
45. Wüthrich, K. (1986) *NMR of proteins and nucleic acids*, Wiley, New York.
46. Damberg, P., Jarvet, J., and Gräslund, A. (2001) *Methods Enzymol. 339*, 271−285.
47. Blondelle, S. E., Lohner, K., and Aguilar, M. (1999) *Biochim. Biophys. Acta 1462*, 89−108.
48. Montserret, R., McLeish, M. J., Bockmann, A., Geourjon, C., and Penin, F. (2000) *Biochemistry 39*, 8362−8373.

49. Lindberg, M., Jarvet, J., Langel, U., and Graslund, A. (2001) *Biochemistry 40*, 3141−3149.
50. Zhou, N. E., Zhu, B. Y., Sykes, B. D., and Hodges, R. S. (1992) *J. Am. Chem. Soc. 114*, 4320−4326.
51. Daggett, V., Kollman, P. A., and Kuntz, I. D. (1991) *Biopolymers 31*, 1115−1134.
52. Bechinger, B. (1999) *Biochim. Biophys. Acta 1462*, 157−183.
53. Gesell, J., Zasloff, M., and Opella, S. J. (1997) *J. Biomol. NMR 9*, 127−135.
54. Segrest, J. P., De Loof, H., Dohlman, J. G., Brouillette, C. G., and Anantharamaiah, G. M. (1990) *Proteins 8*, 103−117.

BI034401D